A Journal of the Gesellschaft Deutscher Chemiker

Angewandte International Edition

GDCh

Chemie

www.angewandte.org

Accepted Article

Title: Single-Atom Nanozyme for Wound Antibacterial Applications

Authors: Bolong Xu, Hui Wang, Weiwei Wang, Lizeng Gao, Shanshan Li, Xueting Pan, Hongyu Wang, Hailong Yang, Xiangqin Meng, Qiuwen Wu, Lirong Zheng, Shenming Chen, Xinghua Shi, Kelong Fan, Xiyun Yan, and Huiyu Liu

To be cited as: *Angew. Chem. Int. Ed.* 10.1002/anie.201813994
Angew. Chem. 10.1002/ange.201813994

Link to VoR: http://dx.doi.org/10.1002/anie.201813994
http://dx.doi.org/10.1002/ange.201813994

WILEY-VCH

10.1002/anie.201813994

WILEY-VCH

COMMUNICATION

Single-Atom Nanozyme for Wound Antibacterial Applications

Bolong Xu,[+] Hui Wang,[+] Weiwei Wang,[+] Lizeng Gao, Shanshan Li, Xueting Pan, Hongyu Wang, Hailong Yang, Xiangqin Meng, Qiuwen Wu, Lirong Zheng, Shenming Chen, Xinghua Shi, Kelong Fan,* Xiyun Yan,* and Huiyu Liu*

Abstract: The single-atom catalysts (SACs) as homogeneous catalysts have been widely explored for chemical catalysis. However, few studies focus on SACs' applications in enzymatic catalysis. Herein, we first report that a zinc-based zeolitic−imidazolate-frameworks (ZIF-8) derived carbon nanomaterial containing atomically dispersed zinc atoms could serve as a highly efficient single-atom peroxidase mimic. To reveal its structure-activity relationship, we systematically investigated the structural evolution of SAzyme. In addition, the coordinatively unsaturated active zinc sites and catalytic mechanism of SAzyme are disclosed using density functional theory (DFT) calculations. The SAzyme with high therapeutic effect and biosafety shows great promises for wound antibacterial applications.

Since the first evidence of Fe_3O_4 nanoparticles as peroxidase mimetics was reported in 2007,[1] ever-growing interests have been devoted to mimicking natural enzymes. Various nanomaterials, including metal oxides, noble metals, and carbon nanomaterials have been identified harboring intrinsic enzyme-like activities.[2] They possess considerable potential for a wide range of applications, such as immunoassays,[3] biosensors,[4] antibacterial and antibiofilm agents.[5] Despite significant progress having been made, it remains a big challenge to control the biocatalytic sites of nanozymes due to the inhomogeneity in the construction of traditional nanozymes.

Recently, single-atom catalysts (SACs) containing atomically dispersed metal active sites have become a new frontier in catalysis field due to their maximum metallic atom utilization, high activity and selectivity.[6] M−N−C (M refers to Fe, Co, Mn, etc.) SACs, which derive from transition-metal-containing macrocycles, possess similar $M-N_x$ sites with natural metalloenzymes. Therefore, it is hypothesized that M−N−C SACs can serve as bioinspired single-atom nanozymes (SAzymes) to mimic the structure and catalytic activity of natural enzymes. Importantly, it is easy to identify atomically dispersed metal active sites of SAzymes, which will benefit the understanding of the structure-property of nanozymes. However, in comparison with the extensive applications in electrocatalysis,[7] photocatalysis,[8] and organic conversion,[9] SACs have rarely been explored for biocatalysis,[10] let alone revealed their enzymatic catalytic mechanism.

In our previous studies,[11] we demonstrate that the monodispersed ZIF-8 (Figure 1a) derived carbon nanospheres containing zinc-centered porphyrin-like structure (denoted as "PMCS") (Figure 1b) can act as photosensitizer and sonosensitizer, showing great promises in tumor therapy. In this work, inspired by the fact that zinc metalloenzymes can also directly participate in biological catalysis,[12] we first demonstrate that PMCS containing atomically dispersed active single zinc atoms can serve as a SAzyme with the excellent peroxidase-like activity, exhibiting enhanced *in vitro* antibacterial effect with an inhibition rate of up to 99.87% on *P. aeruginosa* and significantly promoting wound healing. The high peroxidase-like activity of SAzyme is found to be attributed to the coordinatively unsaturated $Zn-N_4$ sites, resulting in the decomposition of hydrogen peroxide (H_2O_2) and the formation of hydroxyl radicals (•OH). We believe this work opens a new horizon for the exploration of SACs in enzymatic catalysis field and bioapplications.

PMCS were fabricated by using ZIF-8 as precursor *via* mesoporous silica ($mSiO_2$)-protected pyrolysis strategy (pyrolysis temperature of 800 °C) according to the reported method.[11b] The morphology and size distributions were characterized by transmission electron microscopy (TEM) and dynamic light scattering (DLS). Both ZIF-8 and PMCS exhibited uniform size distributions with an average diameter of ~130 nm (Figure 1c-e and Figure S1). The mapping images and energy dispersive spectrum (EDS) showed a uniform distribution of C, O, N and Zn elements over the entire architecture of PMCS (Figure 1f and Figure S2). The atomically dispersed single zinc atoms identified by isolated bright dots were detected by high-angle annular dark-field scanning transmission electron microscope (HAADF-STEM) (Figure 1g,h). In addition, the presence of both Zn and N elements was confirmed by electron energy loss spectrum (EELS). Two peaks at ~1040 and 401 eV are assigned to the characteristic Zn $L_{2,3}$ edges and N K edges, respectively,[13] indicating the formation

[*] B. Xu, Dr. W. Wang, S. Li, X. Pan, H. Y. Wang, H. Yang, Prof. H. Liu
Beijing Advanced Innovation Center for Soft Matter Science and Engineering, State Key Laboratory of Organic-Inorganic Composites
Bionanomaterials & Translational Engineering Laboratory
Beijing Key Laboratory of Bioprocess
Beijing Laboratory of Biomedical Materials
Beijing University of Chemical Technology
Beijing 100029, China
E-mail: liuhy@mail.buct.edu.cn
Dr. H. Wang, Prof. X. Shi
CAS Key Laboratory of Nanosystem and Hierarchial Fabrication
CAS Center for Excellence in Nanoscience
National Center for Nanoscience and Technology
Beijing 100190, China
Q. Wu, Prof. L. Gao
Institute of Translational Medicine
Department of Pharmacology
School of Medicine, Yangzhou University
Yangzhou, Jiangsu 225001, China
X. Meng, Dr. K. Fan, Prof. X. Yan
Key Laboratory of Protein and Peptide Pharmaceuticals
Institute of Biophysics
Chinese Academy of Sciences
Beijing 100101, China
E-mail: fankelong@ibp.ac.cn; yanxy@ibp.ac.cn
Dr. L. Zheng
Beijing Synchrotron Radiation Facility
Institute of High Energy Physics
Chinese Academy of Sciences
Beijing 100049, China
Prof. S. Chen
Department of Chemical Engineering and Biotechnology
National Taipei University of Technology
Taipei, Taiwan 106 (ROC)
[+] These authors contributed equally to this work.

Supporting information for this article is given via a link at the end of the document. ((Please delete this text if not appropriate))

10.1002/anie.201813994

of Zn–N_x bonding (Figure 1i). The Zn content in PMCS was quantified to be 3.12 wt% by inductively coupled plasma optical emission spectrometry (ICP-OES). After high-temperature pyrolysis, PMCS showed only two characteristic (002) and (101) diffraction peaks of graphitic carbon with 2θ at ~26° and 45°, respectively (Figure S3). No peaks corresponding to ZnO or metallic Zn were observed, excluding the presence of large crystalline particles of Zn-containing species.

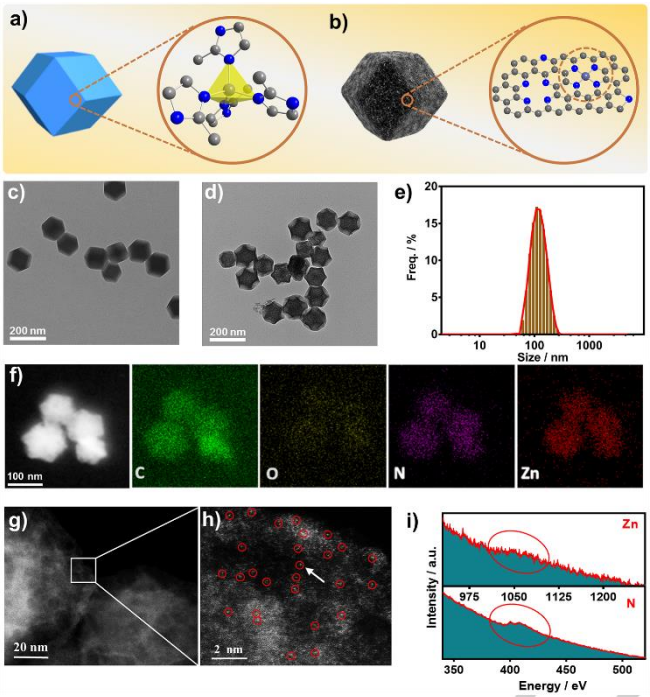

Figure 1. a) ZIF-8 and its corresponding ZnN_4 tetrahedral structural framework; b) PMCS and their corresponding porphyrin-like structural model; TEM images of c) ZIF-8 and d) PMCS; e) Size distributions of PMCS determined by DLS; f) Elemental mapping of PMCS; g, h) Sub-angstrom resolution HAADF-STEM images of PMCS, partial single zinc atoms are tagged by red circles; i) EELS spectra of Zn and N elements from the bright dots shown by the white arrow in (h).

First, the peroxidase-like activity of PMCS was systematically evaluated in the catalytic oxidation of 3, 3′, 5, 5′-tetramethylbenzidine (TMB). Results showed that PMCS effectively catalyzed the oxidation of TMB in the presence of H_2O_2 in concentration, pH and temperature-dependent manners (Figure 2a and Figure S4). The optimal pH and temperature were approximately 4.5 and 45 °C, which are similar to those (4.5 and 35 °C) of natural horseradish peroxidase (HRP).[1] Figure S5 demonstrated that PMCS remained high catalytic stability over a wide range of pH and temperature. To analyze the catalytic activity of PMCS, we obtained the Michaelis-Menten constant (K_M) (Figure 2b,c). K_M, which represent the affinity of substrates to the enzyme, were determined as 40.16 mM for H_2O_2 substrate and 0.224 mM for TMB substrate (Table S1), indicating the comparable affinity of PMCS for H_2O_2 and TMB substrate with natural HRP. In addition, PMCS exhibited markedly higher peroxidase-like activity compared with extensively studied Fe_3O_4 nanozyme and other carbon materials (graphitic carbon nitride and graphene oxide) under same reaction condition in our qualitative analysis experiments (Figure S6 and S7), indicating that PMCS could act as an efficient single-atom peroxidase mimic.

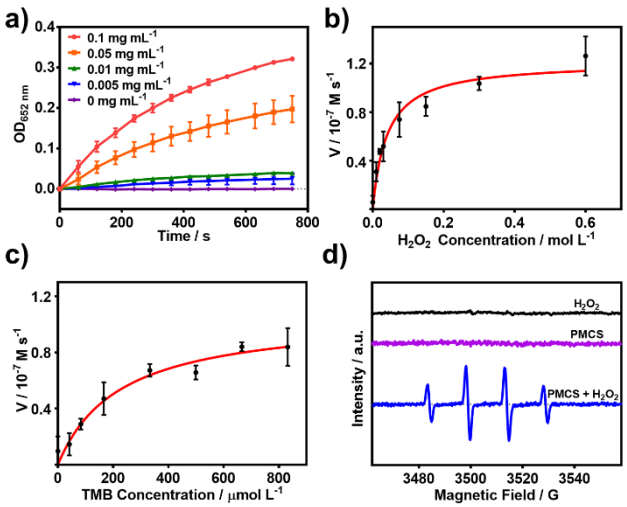

Figure 2. a) Peroxidase-like activity of PMCS with different concentrations; steady-state kinetic assay of PMCS for b) H_2O_2 and c) TMB, respectively; d) ESR spectra demonstrating •OH generation by H_2O_2, PMCS, and PMCS + H_2O_2.

As known, •OH can cause the oxidation of cellular components, thus inducing the bacteria apoptosis.[14] Therefore, it is important to determine the generation of •OH by nanozyme. Electron spin resonance (ESR) spectra demonstrated that when adding 100 μM H_2O_2 into PMCS system, amounts of •OH were identified (Figure 2d). Meanwhile, ESR signal intensity of •OH in PMCS increased by 29.15% when compared with that in Fe_3O_4 under the same particle numbers (Figure S8 and Table S2). These results suggested that PMCS could induce the generation of •OH by catalyzing the decomposition of H_2O_2, which was similar to the behavior of HRP in the H_2O_2/HRP/DMPO (DMPO: 5, 5′-dimethyl-1-pyrroline N-oxide) system.[15]

To understand the origin of the high peroxidase-like activity, we first investigated the pyrolysis temperature's effect on the structure-activity relationship of PMCS. Carbonized ZIF-8 derived nanomaterials were prepared under the pyrolysis temperature of 600, 700, 900 and 1000 °C, respectively (denoted as "c-ZIF-600", "c-ZIF-700", "c-ZIF-900" and "c-ZIF-1000", respectively). Compared with PMCS, c-ZIF-600 and c-ZIF-700 didn't show significant peroxidase-like activities, indicating no formation of enough active sites, while c-ZIF-900 and c-ZIF-1000 were also found to exhibit low peroxidase-like activities (Figure S9). TG/DSC spectrum showed that ZIF-8 began to phase change at ~600 °C (Figure S10). Raman spectra in Figure S11 indicated that PMCS showed only two characteristic peaks of D and G bands of carbon materials with an I_D / I_G value of 0.97, indicating a high degree of graphitization. The D and G band represent the numerous structural defects and the existence of the graphitic

10.1002/anie.201813994

structure, respectively.[16] The increased I_D / I_G ratio demonstrated the formation of more defect sites.[16] The defect is capable of facilitating the interfacial electron transfer between catalyst and reactant,[17] which could partially account for the excellent catalytic activity of PMCS SAzyme.

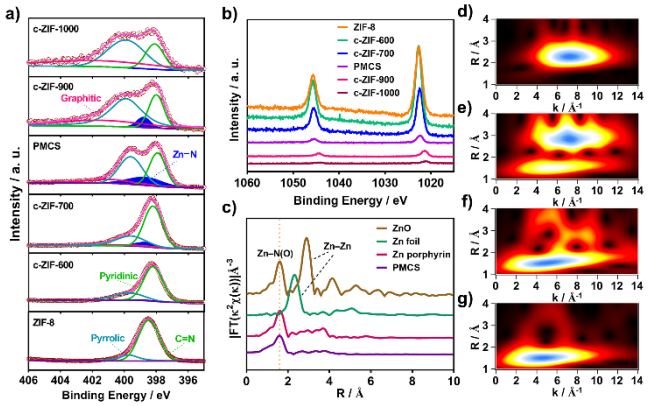

Figure 3. High-resolution a) N 1s and b) Zn 2p XPS spectra for c-ZIF-1000, c-ZIF-900, PMCS, c-ZIF-700, c-ZIF-600 and ZIF-8; c) Zn K-edge EXAFS spectra for ZnO, Zn foil, Zn porphyrin and PMCS; WT of Zn K-edge EXAFS for d) Zn foil, e) ZnO, f) Zn porphyrin and g) PMCS.

X-ray photoelectron spectroscopy (XPS) measurements were performed to further the reveal structure-activity relationship of PMCS. Figure S12 and Table S3 indicated that the presence of C, O, N, and Zn elements for all samples. With the increasing carbonization temperature, both the N and Zn contents gradually declined while the C content increased due to the formation of graphitic carbon (Figure S13 and Table S3). Despite a decrease of N content for PMCS, the amount of N was still sufficient for forming Zn–N_x sites considering the relatively low zinc content and atomic ratio of Zn:N (0.066) (Table S4). In the N 1s XPS spectra (Figure 3a), a sharp peak at 398.5 eV assigning to C=N of 2-methylimidazole was observed for ZIF-8.[18] After high-temperature pyrolysis, a peak at 401.2 eV for PMCS was attributed to graphitic N, which can affect electronic structure of carbon and promote catalytic activity of PMCS.[19] Moreover, the N 1s XPS peak at 398.7 eV assigned to Zn–N.[20] The percentage of Zn–N gradually increased from 1.30% (for c-ZIF-600) to 16.24% (for PMCS), then decreased to 2.26% (for c-ZIF-1000) due to the evaporation of Zn at high temperature,[21] indicating the presence of large amounts of Zn–N_x sites for PMCS (Table S5). In addition, the binding energy of the Zn 2p in PMCS had a ~0.4 eV shift towards low energy compared with ZIF-8 (Figure 3b). A noticeable auger line shift by 1.6 eV towards low energy from ZIF-8 to PMCS in Zn KLL auger lines was also detected (Figure S14). The lower binding energy demonstrated that the electron cloud density around the Zn atoms in PMCS increased, leading to a positive effect on the electron transfer between PMCS SAzyme and substrates. These results demonstrated that the high catalytic activity of PMCS was mainly attributed to the presence of single zinc sites.

To further confirm the structure of PMCS in atomic level, extended X-ray absorption fine structure (EXAFS) analysis was performed. Figure 3c showed the Fourier-transformed (FT) k^3-weighted EXAFS spectra at the Zn-K edge. Compared with the references samples, PMCS exhibited only one main peak at ≈ 1.6 Å, corresponding to the Zn–N (O) scattering paths, while no Zn–Zn peak was observed. Wavelet transform (WT) of Zn-K edge oscillations was used to further identify the atomically dispersion of zinc atoms. The WT maximum at ≈ 5.0 Å for PMCS indicated the presence of Zn–N (O) bonding, no WT maximum corresponding to Zn–Zn was observed (Figure 3d-g). These results confirmed that Zn species in PMCS were atomically dispersed, which is consistent with the above HAADF-STEM result. EXAFS fitting was performed to obtain the coordination configuration of single zinc atoms of PMCS. Best fitting results were presented in Figure S15. The bond length was 2.02 Å and the coordination number of zinc was ≈ 4.6 (Table S6). Combining with the above results and analysis, we can conclude that isolated zinc atoms were atomically dispersed in a carbon matrix and were four-fold coordinated by N atoms. Moreover, N or O atoms were considered to be absorbed on partial zinc atoms in perpendicular to Zn–N_4 plane, resulting in an average coordination number of 4.6.

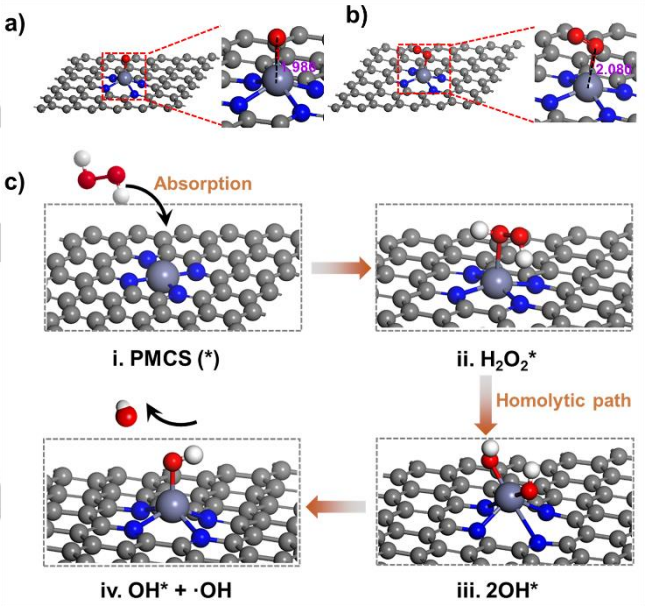

Figure 4. a, b) Optimized structures of O and O_2 species adsorbed on the surface of PMCS, respectively. Interatomic distances are presented in Å; c) Proposed catalytic mechanism schematics of PMCS. The dark slate blue, blue, gray, red and white balls represent the Zn, N, C, O and H atoms, respectively.

The coordinatively unsaturated metal atoms play an important role in single-atom catalysis.[9, 22] Thus, density functional theory (DFT) calculations were performed to investigate the unsaturated coordination structure of single zinc atoms. As shown in Figure 4a,b, when performing the adsorption models of O and O_2, PMCS with five-coordinated structure can stably exist, with a Zn–O bond length of 1.986 and 2.080 Å, respectively. Then we investigated the effect of the fifth ligand N atom for activating the H_2O_2 over PMCS. Results showed that pyrrolic N and pyridinic N as fifth ligand N species lead to a negative effect on the activation the H_2O_2 (Figure S16). The similar negative impact was also observed for the adsorption models of O and O_2 with a large Zn–O bond length of 3.015 and 3.307 Å, respectively (Figure S17). These

10.1002/anie.201813994

results indicated that six-coordinated structure in PMCS could not stably exist, which is quite different from that in reported Fe–N_4 moiety (Figure S18).[22] Therefore, we concluded that the maximum coordination number of single zinc sites in PMCS is 5. Only the unsaturated four-coordinated structure is active despite the average coordination number of PMCS being 4.6 determined by EXAFS fitting. Then we proposed a possible catalytic mechanism by DFT calculations. First, the H_2O_2 molecule was absorbed on Zn–N_4 active site in PMCS (**i**) with an adsorption energy of −0.45 eV (**ii**). The activated H_2O_2 molecules easily dissociated by homolytic path, resulting in the generation of 2OH* (**iii**). Then a hydroxyl group desorbed from single zinc site, leading to the generation of an active hydroxyl radical and OH* (**iv**). The reaction energy from step (**i**) →(**iv**) was 0.24 eV. The low reaction energy could be easily overcome at room temperature (Figure 4c, Figure S19 and S20). Finally, Zn–OH returned to its initial state (**i**) after reacting with other substrates under acidic condition.[23] In addition, the heterolytic path of H_2O_2 was also studied. Our tests showed that the energy barrier for the heterolytic path of H_2O_2* to O*_H_2O* was much higher than that for the homolytic path of H_2O_2* to 2OH*, indicating that the latter one was more favored kinetically. The reaction energies for the two paths were calculated to be −0.41 and −0.70 eV, respectively (Figure S21). Therefore, PMCS containing single zinc active sites can effectively induce the generation of •OH by catalyzing the decomposition of H_2O_2, resulting in high peroxidase-like activity.

Encouraged by the high peroxidase-like activity of PMCS SAzyme, the *in vitro* and *in vivo* experiments were performed to evaluate the antibacterial effect of PMCS SAzyme. First, Figure S22 showed that PMCS SAzyme exhibited good biocompatibility with little leakage of Zn^{2+}, which guaranteed its *in vivo* applications.

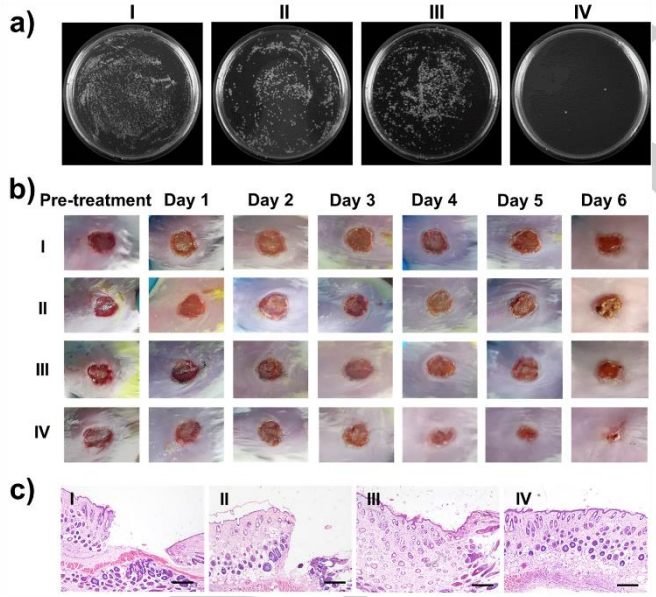

Figure 5. a) Photographs of bacterial colonies formed by *P. aeruginosa* after exposed to (I) NaAc buffer, (II) NaAc buffer + H_2O_2, (III) PMCS and (IV) PMCS + H_2O_2, the final working concentrations for NaAc buffer, H_2O_2 and PMCS are 0.1 M, 100 μM and 100 μg mL^{-1}, respectively; b) Photographs of *P. aeruginosa* infected wound treated with (I)-(IV) at different days; c) Histologic analysis of the wounds for (I)-(IV) after 6 days of therapy, scale bar is 500 μm.

For *in vitro* antibacterial experiments, the plate count method was utilized to determine the antibacterial ability of PMCS against *P. aeruginosa* (Figure 5a, Figure S23 and S24). In the presence of H_2O_2, PMCS showed the extremely high antibacterial effect on *P. aeruginosa* with an inhibition rate of up to 99.87% compared with c-ZIF-600, c-ZIF-700, c-ZIF-900 and c-ZIF-600. The bacterial morphology was characterized by field emission scanning electron microscopy (FE-SEM) (Figure S25). Results showed that PMCS tightly bound to bacteria, and when the bacteria incubated with PMCS and H_2O_2 together, the bacterial morphology became flat and bacteria surface became rough. We further analyzed the apoptosis of the treated bacteria by propidium iodide (PI) staining (Figure S26). Compared with control, the ratio of bacteria apoptosis in PMCS treated group dramatically increased. These results indicated that PMCS disrupted bacterial membrane and induced bacterial apoptosis.

The *in vivo* bactericidal efficacy of PMCS was further evaluated. Wound infection model was established using *P. aeruginosa* to infect wound in mice. Mice treated with PMCS and low concentration of H_2O_2 (100 μM) effectively promoted wound healing (Figure 5b). The PMCS + H_2O_2 treated mice took 6 days to achieve complete wound-healing, while the controls took more than 11 days. The infected wound healing efficiency was further verified by histological staining (Figure 5c). After treatment, the mice of PMCS + H_2O_2 group were sacrificed to perform toxicological analysis of main organs (Figure S27). No obvious toxicity was detected for the primary organs, indicating PMCS exhibited reasonable *in vivo* biosafety. Therefore, PMCS SAzyme exhibits both high therapeutic effect and biosafety for wound disinfection and healing.

In summary, we for the first time presented an efficient SAzyme with excellent peroxidase-like activity by using ZIF-8 derived Zn−N−C SAC. The PMCS SAzyme possesses similar catalytic activity and M−N_x active sites with natural enzymes. We confirmed that the high catalytic activity of PMCS SAzyme was attributed to the coordinatively unsaturated Zn−N_4 active sites. In addition, a possible catalytic mechanism was revealed by DFT calculations. The inhibition rate of PMCS on *P. aeruginosa* was as high as 99.87%. In *in vivo* infected wound model, PMCS SAzyme significantly promoted wound healing without significant toxicity to various tissues and organs. We believe this work will advance the development of different SACs in biocatalysis field.

Acknowledgements

This work was supported by the National Natural Science Foundation of China (No. 21822802, 81671810, 51772018, 51572271, 31871005 and 31530026), the National Basic Research Program of China (973 Program) under Grant No. 2016YFA0201500, the Fundamental Research Funds for the Central Universities (buctrc201610, PYBZ1705, ZY1711 and XK1802-8), the Young Elite Scientist Sponsorship Program by CAST (2015QNRC001), the Key Research Program of Frontier Sciences (Grant No. QYZDB-SSW-SMC013), and the Strategic Priority Research Program (Grant No. XDB29040101), CAS.

Keywords: single-atom nanozyme • unsaturated Zn–N_4 sites • peroxidase-like activity • antibacterial effect

[1] L. Gao, J. Zhuang, L. Nie, J. Zhang, Y. Zhang, N. Gu, T. Wang, J. Feng, D. Yang, S. Perrett, X. Yan, *Nat. Nanotechnol.* **2007**, *2*, 577-583.

[2] Y. Hu, X. J. Gao, Y. Zhu, F. Muhammad, S. Tan, W. Cao, S. Lin, Z. Jin, X. Gao, H. Wei, *Chem. Mater.* **2018**, *30*, 6431-6439; J. Wu, X. Wang, Q. Wang, Z. Lou, S. Li, Y. Zhu, L. Qin, H. Wei, *Chem. Soc. Rev.* **2019,** DOI: 10.1039/C8CS00457A.

[3] H. Wei, E. Wang, *Chem. Soc. Rev.* **2013**, *42*, 6060-6093.

[4] a) B. Liu, Z. Huang, J. Liu, *Nanoscale* **2016**, *8*, 13562-13567; b) Q. Wang, X. Zhang, L. Huang, Z. Zhang, S. Dong, *ACS Appl. Mater. Interfaces* **2017**, *9*, 7465-7471.

[5] a) Y. Tao, E. Ju, J. Ren, X. Qu, *Adv. Mater.* **2015**, *27*, 1097-1104; b) W. Yin, J. Yu, F. Lv, L. Yan, L. R. Zheng, Z. Gu, Y. Zhao, *ACS nano* **2016**, *10*, 11000-11011; c) Z. Chen, H. Ji, C. Liu, W. Bing, Z. Wang, X. Qu, *Angew. Chem. Int. Ed.* **2016**, *55*, 10732-10736; d) K. Herget, P. Hubach, S. Pusch, P. Deglmann, H. Götz, T. E. Gorelik, I. y. A. Gural'skiy, F. Pfitzner, T. Link, S. Schenk, *Adv. Mater.* **2017**, *29*, 1603823.

[6] a) H. Zhang, G. Liu, L. Shi, J. Ye, *Adv. Energy Mater.* **2018**, *8*, 1701343; b) Z. Chen, E. Vorobyeva, S. Mitchell, E. Fako, M. A. Ortuño, N. López, S. M. Collins, P. A. Midgley, S. Richard, G. Vilé, *Nat. Nanotechnol.* **2018**, *13*, 702; c) J. Liu, *ACS Catal.* **2016**, *7*, 34-59.

[7] Y. Chen, S. Ji, C. Chen, Q. Peng, D. Wang, Y. Li, *Joule* **2018**, *2*, 1242-1264.

[8] X. Fang, Q. Shang, Y. Wang, L. Jiao, T. Yao, Y. Li, Q. Zhang, Y. Luo, H. L. Jiang, *Adv. Mater.* **2018**, *30*, 1705112.

[9] W. Liu, L. Zhang, X. Liu, X. Liu, X. Yang, S. Miao, W. Wang, A. Wang, T. Zhang, *J. Am. Chem. Soc.* **2017**, *139*, 10790-10798.

[10] W. Ma, J. Mao, X. Yang, C. Pan, W. Chen, M. Wang, P. Yu, L. Mao, Y. Li, *Chem. Commun.* **2018**, DOI: 10.1039/C8CC08116F.

[11] a) X. Pan, L. Bai, H. Wang, Q. Wu, H. Wang, S. Liu, B. Xu, X. Shi, H. Liu, *Adv. Mater.* **2018**, *30*, e1800180; b) S. Wang, L. Shang, L. Li, Y. Yu, C. Chi, K. Wang, J. Zhang, R. Shi, H. Shen, G. I. Waterhouse, S. Liu, J. Tian, T. Zhang, H. Liu, *Adv. Mater.* **2016**, *28*, 8379-8387.

[12] a) P. Bhyrappa, U. Sarangi, B. Varghese, *Inorg. Chim. Acta* **2015**, *426*, 171-182; b) G. Miyazaki, H. Morimoto, K.-M. Yun, S.-Y. Park, A. Nakagawa, H. Minagawa, N. Shibayama, *J. Mol. Biol.* **1999**, *292*, 1121-1136; c) A. A. Ensign, I. Jo, I. Yildirim, T. D. Krauss, K. L. Bren, *Proc. Natl. Acad. Sci. USA* **2008**, *105*, 10779-10784.

[13] T. Mizoguchi, M. Yoshiya, J. Li, F. Oba, I. Tanaka, H. Adachi, *Ultramicroscopy* **2001**, *86*, 363-370.

[14] L. Gao, K. M. Giglio, J. L. Nelson, H. Sondermann, A. J. Travis, *Nanoscale* **2014**, *6*, 2588-2593.

[15] C. Rota, C. F. Chignell, R. P. Mason, *Free Radical Biol. Med.* **1999**, *27*, 873-881.

[16] F. Zheng, Y. Yang, Q. Chen, *Nat. Commun.* **2014**, *5*, 5261.

[17] G. Zhang, M. Zhang, X. Ye, X. Qiu, S. Lin, X. Wang, *Adv. Mater.* **2014**, *26*, 805-809.

[18] Z. Liu, G. Li, T. Cui, A. Lahiri, A. Borodin, F. Endres, *Phys. Chem. Chem. Phys.* **2017**, *19*, 25989-25995.

[19] H. Zhang, S. Hwang, M. Wang, Z. Feng, S. Karakalos, L. Luo, Z. Qiao, X. Xie, C. Wang, D. Su, Y. Shao, G. Wu, *J. Am. Chem. Soc.* **2017**, *139*, 14143-14149.

[20] P. Song, M. Luo, X. Liu, W. Xing, W. Xu, Z. Jiang, L. Gu, *Adv. Funct. Mater.* **2017**, *27*, 1700802.

[21] a) Y. Chen, S. Ji, S. Zhao, W. Chen, J. Dong, W.-C. Cheong, R. Shen, X. Wen, L. Zheng, A. I. Rykov, *Nat. Commun.* **2018**, *9*, 5422; b) Y. Z. Chen, C. Wang, Z. Y. Wu, Y. Xiong, Q. Xu, S. H. Yu, H. L. Jiang, *Adv. Mater.* **2015**, *27*, 5010-5016.

[22] D. Deng, X. Chen, L. Yu, X. Wu, Q. Liu, Y. Liu, H. Yang, H. Tian, Y. Hu, P. Du, *Sci. Adv.* **2015**, *1*, e1500462.

[23] a) K. Herget, P. Hubach, S. Pusch, P. Deglmann, H. Gotz, T. E. Gorelik, I. A. Gural'skiy, F. Pfitzner, T. Link, S. Schenk, M. Panthofer, V. Ksenofontov, U. Kolb, T. Opatz, R. Andre, W. Tremel, *Adv. Mater.* **2017**, *29*; b) I. Celardo, J. Z. Pedersen, E. Traversa, L. Ghibelli, *Nanoscale* **2011**, *3*, 1411-1420.

10.1002/anie.201813994

WILEY-VCH

COMMUNICATION

ZIF-8 derived Zn–N–C single-atom catalyst is considered to be an efficient single-atom nanozyme (SAzyme). The SAzyme containing unsaturated $Zn–N_4$ sites shows excellent peroxidase-like activity and high antibacterial effect on *P. aeruginosa*, and it is proved to be an effective antibacterial agent for wound antibacterial applications.

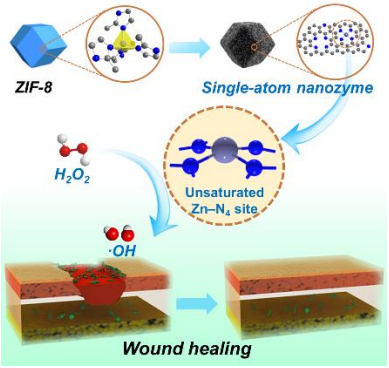

Bolong Xu,⁺ Hui Wang,⁺ Weiwei Wang,⁺ Lizeng Gao, Shanshan Li, Xueting Pan, Hongyu Wang, Hailong Yang, Xiangqin Meng, Qiuwen Wu, Lirong Zheng, Shenming Chen, Xinghua Shi, Kelong Fan, Xiyun Yan,* and Huiyu Liu**

Page No. – Page No.

Single-Atom Nanozyme for Wound Antibacterial Applications